



1 **Bimodal Hydrographs in Semi-humid Forested Watershed: Characteristics and**
2 **Occurrence Conditions**

3 **Zhen Cui¹, Fuqiang Tian^{1*}, Zilong Zhao¹, Zitong Xu¹, Yongjie Duan¹, Jie Wen², Mohd**
4 **Yawar Ali Khan³**

5 ¹ Department of Hydraulic Engineering & State Key Laboratory of Hydrosience and
6 Engineering, Tsinghua University, Beijing 100084, China.

7 ² State Key Laboratory of Simulation and Regulation of Water Cycle in River Basin, China
8 Institute of Water Resources and Hydropower Research, Beijing 100038, China.

9 ³ Department of Hydrogeology, Faculty of Earth Sciences, King Abdulaziz University,
10 Jeddah 21589, Saudi Arabia.

11

12 Corresponding to: Fuqiang Tian (tianfq@tsinghua.edu.cn)

13 **Key Points:**

- 14
- 15 • The stormflow hydrograph of the studied watershed displays a bimodal pattern.
 - 16 • The onset of the bimodal response demonstrates a threshold behavior.
 - 17 • Delayed stormflow is mainly contributed by shallow groundwater.



18 **Abstract**

19 Bimodal runoff behavior, characterized by two distinct peaks in flow response, often leads to
20 significant stormflow and associated flooding. Understanding and characterizing this phenomenon
21 is crucial for effective flood forecasting. However, this runoff behavior has been understudied and
22 poorly understood in semi-humid regions. In this study, we investigated the response
23 characteristics and occurrence conditions of bimodal hydrograph based on the hydrometric and
24 isotope data spanning 10 years in a semi-humid forested watershed in North China. The main
25 findings include: 1) the onset of the bimodal hydrograph exhibits a threshold behavior, with
26 delayed streamflow peaks occurring when the sum of event rainfall (P) and antecedent soil
27 moisture index prior to the rainfall (ASI) exceeds 200 mm; 2) isotopic hydrograph separation
28 reveals that delayed stormflow process is primarily driven by pre-event water, with increasing
29 contributions of pre-event water during catchment wetting-up; 3) the dynamic variation in
30 groundwater level precedes that of streamflow, establishing a hysteretic relationship wherein
31 groundwater level peaks before streamflow during delayed stormflow. These findings, supported
32 by onsite observations, emphasize the dominance of shallow groundwater flow in the generation
33 of delayed stormflow.

34 **Keywords:** Semi-humid watershed, Stormflow, Bimodal runoff response, Threshold, Shallow
35 groundwater

36 **1. Introduction**

37 Runoff generation is one of the most complex hydrological processes due to their complexity
38 and non-linearity (McDonnell *et al.*, 2007; McGuire & McDonnell, 2010; Phillips, 2003). At



39 different times of a year, the activation of different runoff generating mechanisms, and contrasting
40 compartments and flow routes form different hydrograph shapes, which are generally classified as
41 unimodal and bimodal response types (Jenkins *et al.*, 1994; Gu, 1996; Kosugi *et al.*, 2011). A
42 unimodal response is characterized by a needle-shaped peak which responds immediately to the
43 rainfall impulse. In contrast, the bimodal response contains a delayed damped arch-shaped peak
44 responding to the same rainfall impulse in addition to the direct peak (Martínez-Carreras *et al.*,
45 2016). Generally, the delayed peak in a bimodal event contributes substantially more runoff than
46 the first peak (Zillgens *et al.*, 2007). For instance, the study by Onda *et al.* (2001) showed that the
47 delayed peak discharge is five to ten times greater than the first peak. When the bimodal runoff
48 event occurs, the streamflow increases markedly and lasts for several days. Therefore,
49 characterizing the bimodal response is of great significance to understanding the runoff generation
50 process and essential to achieving improved forecasting of extreme floods.

51 Since the bimodal hydrograph was accidentally observed in Côte d'Ivoire in 1960 during flood
52 frequency analysis and surface runoff generation study (Dubreuil, 1960, 1985), bimodal response
53 has piqued the interest of many hydrologists worldwide and been recorded in watersheds with
54 varied geological and climate conditions. For example, Onda *et al.* (2001) observed bimodal
55 hydrographs in a steep mountainous watershed underlain by shale and serpentinite in Japan (annual
56 precipitation: 1800 mm). Padilla *et al.* (2014, 2015) found delayed peaks after the rainfall in a
57 steep headwater catchment underlain by fractured bedrock also in Japan (annual precipitation:
58 2669 mm). Zillgens *et al.* (2007) recorded a delayed peak after the direct peak in Saalach basin in
59 the Austrian Alps (annual precipitation: 1400 mm). Masiyandima *et al.* (2003) found bimodal
60 responses in an inland valley watershed with wet lowlands in central Côte d'Ivoire (annual rainfall:
61 1045 mm). Anderson and Burt (1977, 1978) observed delayed peak after the storm at Bicknoller



62 Combe in Sommerset, composed of impermeable Old Red Sandstone. The characteristics and
63 conditions of occurrence of bimodal hydrograph can provide an effective method for simplifying
64 the description of complex hydrological systems, and comparing stormflow generation mechanism
65 in different watersheds (Tromp-van Meerveld & McDonnel, 2006). However, most of these studies
66 mentioned above have been done in humid regions with rainfall of more than 1000 mm. To the
67 best of authors' knowledge, very few studies if not none have been conducted in semi-humid
68 environment with rainfall less than 800 mm.

69 Meanwhile, recognizing the pivotal role of bimodal response in runoff generation, researchers
70 have made concerted efforts over the past several decades to quantify its characteristics and
71 establish statistical metrics for identifying the occurrence of bimodal events. Findings suggest that
72 indicators for bimodal response encompass factors such as rainfall amount (Haga *et al.*, 2005),
73 pre-event streamflow (Graeff *et al.*, 2009), soil moisture (Anderson & Burt, 1978; Weyman, 1970),
74 groundwater level (Padilla *et al.*, 2015) and storage (Martínez-Carreras *et al.*, 2016). Taking the
75 work of Martínez-Carreras *et al.* (2016) as an illustrative example, it revealed that the delayed peak
76 manifested only when the watershed storage reached a critical threshold of 113 mm. It is
77 noteworthy that predictors vary significantly among watersheds, with only a limited number of
78 studies presenting quantitative results akin to those reported by Martínez-Carreras *et al.* (2016).
79 Moreover, response timing metrics such as response lag to peak—providing insights into different
80 aspects of water travel time during an event—have received comparatively less attention in the
81 evaluation of threshold effects (Dingman, 2015; Ross *et al.*, 2021).

82 Many studies have delved into the compartments and flow pathways responsible for
83 generating distinct runoff response patterns. The first runoff peaks are attributed to factors such as
84 rainwater directly falling onto the stream channel, rapid flow through preferential paths (Becker



85 & McDonnell, 1998; Martínez-Carreras *et al.*, 2015; Wrede *et al.*, 2015), or saturation-excess
86 overland flow in the riparian zone (Anderson & Burt, 1978; Westhoff *et al.*, 2011). While delayed
87 runoff peaks in bimodal events are primarily linked to subsurface flow processes (Weyman, 1970;
88 Onda *et al.*, 2006; Zillgens *et al.*, 2007; Graeff *et al.*, 2009; Padilla *et al.*, 2015). However, a notable
89 gap exists in the literature, as many studies have focused solely on water flow processes within the
90 soil profile without thoroughly investigating whether subsurface stormflow originates from the
91 soil layer, bedrock layer, or a combination of both.

92 Bimodal responses, representing the nonlinear interplay between runoff and rainfall,
93 inherently showcase the stormflow process in terms of both response timing and magnitude. This
94 intuitive manifestation holds significant implications for advancing runoff modeling (Graeff *et al.*,
95 2009; McDonnell *et al.*, 2007) and enhancing the precision of flash flood forecasting (Zhang *et al.*,
96 2021; Zillgens *et al.*, 2007). In our present study, spanning the years 2014 to 2023, we collected
97 data on rainfall, groundwater levels, soil water content, and streamflow within a semi-humid forest
98 experimental watershed in North China. Our investigation involves characterizing the response
99 magnitude and timing of stormflow to rainfall through hydrograph analysis, while also scrutinizing
100 the composition of the water sources contributing to stormflow. Specifically, we hypothesize that
101 (1) the occurrence of bimodal streamflow responses exhibits a threshold behavior with rainfall and
102 watershed wetness, and (2) the primary source of water for the delayed stormflow is subsurface
103 flow.

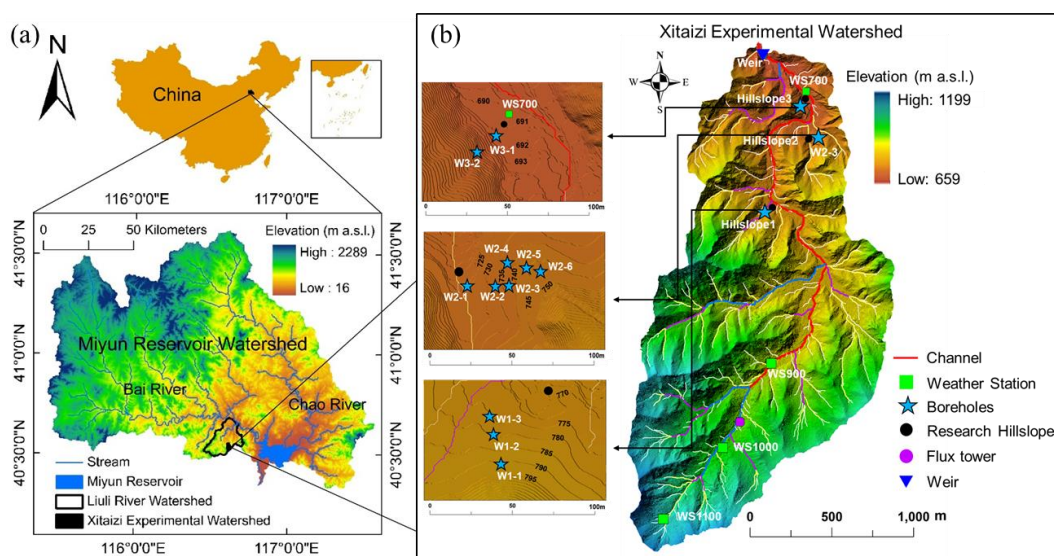


104 2. Materials and Methods

105 2.1 Study area

106 The study headwater catchment, the Xitaizi Experimental Watershed (XEW), is situated at
107 coordinates 40°32'N and 116°37'E, as depicted in Figure 1. Spanning an area of 4.22 km², XEW
108 exhibits elevations ranging from 676 to 1201 m above sea level. Approximately 54% of the area
109 features a slope between 20% and 40%. The region experiences a monsoon-influenced semi-humid
110 climate characterized by an average annual rainfall of 625 mm. The majority of this precipitation,
111 around 80%, occurs between June and September. The annual mean temperature in the area is
112 11.5°C, accompanied by a relative humidity of 59.1%. Experimental and observational activities
113 were conducted over the period from 2014 to 2023.

114





115 **Figure 1.** Location of the Xitaizi Experimental Watershed (XEW) in North China (a), and the
116 detailed distributed monitoring stations and instruments (b), including four automatic weather
117 stations (WS700-1100), one weir, and eleven groundwater boreholes (blue star corresponds with
118 well numbers and locations). Four rain gauges are located near the weather stations, and one is
119 located adjacent to the weir.

120

121 XEW represents a typical location in North China's earth-rocky mountainous region, where
122 approximately 80% of the catchment area is underlain by firmly compacted, deeply weathered
123 granite. Soil mapping and field investigations reveal the prevalent soil types to be brown earth and
124 cinnamon soil (according to Chinese soil taxonomy), with a depth extending to 1.5 meters. The
125 saturated hydraulic conductivity of the soil ranges from 19.5 to 175.3 mm/h, with an average value
126 of 45 mm/h. The bedrock in the area is primarily composed of granite, constituting approximately
127 88% of the total bedrock composition, while gneiss and dolomite are sporadically distributed.
128 Some sections of the granite exhibit fracture, and a layer of regolith is sandwiched between the
129 soil layer and the bedrock layer. In terms of land cover, the catchment is predominantly covered
130 by forest (98%), with 54.2% being broad-leaved, 2.3% coniferous, and 10.5% a mix of coniferous
131 and broad-leaved. The remaining 33% consists of shrubs (Tie *et al.*, 2017).

132 **2.2 Meteorology and runoff measurements**

133 Meteorological variables and runoff have been systematically monitored since 2013.
134 Meteorological conditions were consistently measured using four GRWS100 automatic weather
135 stations (Campbell Scientific, Inc., Logan, UT, USA). These weather stations were strategically
136 distributed quasi-uniformly along the elevation gradient, as depicted in Figure 1. The
137 comprehensive data collection from these stations contributes to a thorough understanding of the
138 meteorological dynamics in the study area over the specified timeframe.



139 For the measurement of air temperature (T_a) and relative humidity at each automatic weather
140 station, an HC2S3-L temperature and relative humidity probe (Rotronic AG, Grindelstrasse,
141 Bassersdorf, Schweiz) was utilized. These probes were equipped with a radiation shield to enhance
142 accuracy. Simultaneously, a LI-190R quantum sensor (LI-COR, Inc., Lincoln, NE, USA) was
143 employed to measure photosynthetically active radiation (PAR). Rainfall data were collected at
144 10-minute intervals using six tipping-bucket rain gauges (Texas Electronics, Inc., Dallas, TX,
145 USA). These gauges were positioned in an open space near the automatic weather stations, and
146 average values were adopted for analysis in this study.

147 Furthermore, the antecedent precipitation index (API), generally used to represent the residual
148 effect of previous precipitation (Mosley, 1979; Iwagami *et al.*, 2010), was calculated for all the
149 events over 3, 6, and 12 days. The API during the antecedent t days is described as follows:

$$150 \quad \text{API}(t) = \sum_{i=1}^t \frac{P_i}{i} \quad (1)$$

151 where i is the day count and P_i is the daily precipitation in the i^{th} day previously.

152 A Parshall flume was installed at the catchment outlet to measure streamflow (Figure 1). The
153 water level in the flume was measured every 5 min with a HOBO capacitance water level logger
154 (Onset, Bourne, Massachusetts, USA) from 2014. Streamflow was calculated using the standard
155 Parshall flume rating curve, and both the rainfall and streamflow measurements were averaged to
156 hourly timesteps, and in this study, the analysis is conducted at hourly timesteps. Unfortunately,
157 the observation equipment is susceptible to failures due to the complex environmental conditions
158 and disturbances caused by wild animals and plants. Compounded by the remote location of XEW,
159 accessing the site promptly to address malfunctions is challenging, leading to the loss of some
160 observation data. Notably, stormflow data from July 19 to August 16, 2016, had to be excluded



161 because the road collapsed during a heavy storm, preventing a significant amount of runoff from
162 passing through the Parshall flume. Furthermore, streamflow data from 2018 to 2019 are
163 unavailable, and the two bimodal events in 2016 were omitted from the hysteresis analysis due to
164 substantial errors in streamflow observations resulting from damage to the diversion channel. The
165 specific observation periods are detailed in Table 1. These limitations underscore the challenges
166 associated with conducting observations in remote and environmentally intricate locations.

167

168

169

170

171 **Table 1.** Rainfall event classification and counts by Year. This table provides a breakdown of the
172 number of rainfall events categorized as unimodal, bimodal, and hybrid bimodal for each year,
173 along with the corresponding time periods. The total counts are summarized at the bottom.

Year	Unimodal event	Bimodal event	Hybrid bimodal event	Time period
2014	7	-	-	Jul 25 - Sep 25
2015	12	2	-	Jun 1 - Oct 1
2016	2	2	1	Jul 10 - Aug 20
2017	-	2	-	Jun 20 - Jul 10
2020	14	2	-	Jul 1 - Oct 10
2021	15	5	2	Jun 1 - Oct 10
2022	18	1	-	Apr 1 - Nov 1
2023	9	-	1	Apr 1 - Nov 1
Total	77	14	4	

174

175 2.3. Soil water content observation

176 Volumetric soil water content (SWC) was measured at eight observation sites using CS616
177 time-domain reflectometry (TDR) probes (Campbell Scientific, Inc., Logan, UT, USA) at 10-min
178 intervals. These measurements were taken at 10-minute intervals. On Hillslope 1, five soil



179 moisture sensors were deployed, with an additional three located adjacent to WS900. These
180 sensors were strategically placed in the soil profiles at 80 cm depth intervals, each at a depth of 10
181 cm. For analysis in this study, the 10-minute interval measurements were aggregated to hourly
182 time steps, and the arithmetic mean of the total SWC across the four profiles was employed.
183 Moreover, SWC data immediately preceding a rainfall event were integrated over the 80 cm depth
184 to calculate an antecedent soil moisture index (ASI), as proposed by Haga *et al.* (2005). This index,
185 commonly utilized in analyzing the impact of antecedent shallow soil water storage on catchment
186 runoff response (Fu *et al.*, 2013; Penna *et al.*, 2011), provides valuable insights into the soil
187 moisture conditions preceding rainfall events.

188 **2.4 Groundwater level observation**

189 Fluctuations in groundwater level (below the ground surface, hereinafter referred to as bgs)
190 were systematically recorded in eleven 80 mm diameter boreholes situated on three hillslopes
191 within the catchment (refer to Figure 1). The boreholes were drilled to depths of 5-26 m in granite
192 (weathered and fractured to varying extents) mantled by thin soils. Unscreened portions of the
193 boreholes accounted for approximately one third to three fifths of the total depth (refer to Table 2).
194 To capture the groundwater level dynamics, HOBO capacitance water level loggers (Onset, USA)
195 were deployed to record water levels in the boreholes at hourly intervals. It is noteworthy that
196 water levels were rarely observed in boreholes W1-1, W1-2, W2-4, W2-5, and W2-6. This
197 observation could be attributed to the boreholes potentially not being drilled deep enough to reach
198 the groundwater, possibly due to challenges encountered during field drilling. Slug tests conducted
199 following installation suggested that the saturated conductivity in the weathered and fractured
200 granite was relatively high, ranging from 5.2×10^{-3} m/day to as high as 1.16 m/day.



201 **Table 2.** Depths and Groundwater Levels of Boreholes. This table summarizes the depths of the
202 bottom and the boundary between unscreened and screened portions, along with the shallowest
203 and deepest groundwater levels of boreholes in the study area.

Borehole	Bottom (m)	Boundary (m)	Shallowest GWL (m)	Deepest GWL (m)
W1-3	10	6	2.8	10 ^a
W2-1	5	2	0.2	2.2
W2-2	10	4	4.8	10 ^a
W2-3	26	9	6.4	12.2
W3-1	10	4	0.8	3.9
W3-2	10	4	6.1	9.9

204 Note: All values indicate depths (in meters) from ground surface; GWL is groundwater level;
205 a indicates the groundwater level dropped below the bottom of the borehole.

206 Note: All values indicate depths (in meters) from the ground surface; GWL represents groundwater
207 level; 'a' indicates the groundwater level dropped below the bottom of the borehole.

208 An index for groundwater level (I_G) was computed by normalizing the groundwater levels in
209 each borehole to their recorded range throughout the research years, following the approach
210 outlined by Detty and McGuire (2010). Subsequently, the arithmetic mean of I_G across all
211 boreholes was calculated, serving as a representative proxy for the groundwater level across the
212 entire catchment. This approach provides a standardized measure that allows for the comparison
213 of groundwater level variations across different boreholes within the study area.

214 2.5 Separation of rainfall events

215 An intensity-based automatic algorithm, as outlined by Tian *et al.* (2012) and Powell *et al.*
216 (2007), was employed to delineate and segregate rainfall events from hourly rainfall time series
217 data. In this algorithm, a threshold rainfall intensity of >0.1 mm/h was utilized to determine the
218 commencement and conclusion of each event, with individual storms being separated by a
219 minimum of six hours. Events characterized by an accumulated rainfall exceeding 5 mm were
220 selected for further analysis. A total of 95 distinct rainfall events, each with a cumulative rainfall
221 of at least 5 mm, were identified and isolated from the rainfall data series spanning the years 2014
222 to 2023, employing the intensity-based automatic method (refer to Table 1).



223 Storm runoff events are identified when streamflow experiences a rapid increase and attains
224 a peak in response to a rain impulse. Throughout the analyses presented, streamflow refers to the
225 total discharge measured at the weir. The separation of stormflow from base flow was achieved
226 using the straight-line separation method, as illustrated in Figure 2. This method involves drawing
227 a line from the hydrograph's initial climb to the point of inflection on the recession limb, following
228 the approach outlined by Zillgens *et al.* (2007). In the context of each event, q_0 is defined as the
229 streamflow before the onset of rainfall. This parameter characterizes the baseflow conditions
230 preceding the hydrograph's response to a rain impulse (Zillgens *et al.*, 2007). The separation of
231 stormflow from base flow allows for a more detailed examination of the runoff dynamics during
232 distinct rainfall events.

233 **2.6 Hydrograph and event types**

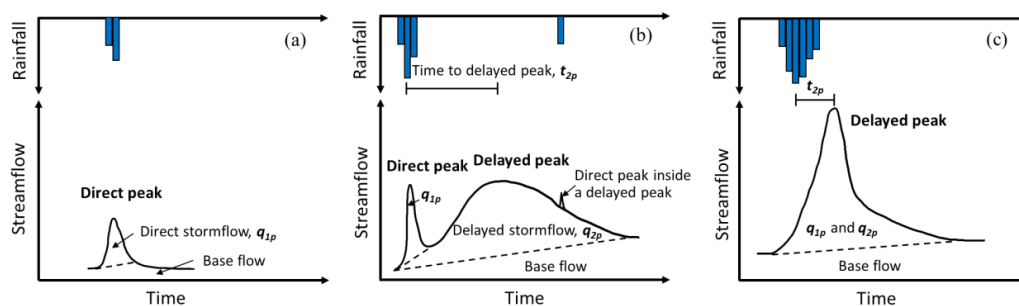
234 The hydrograph served as a valuable tool for characterizing the timing, magnitude, and
235 duration of runoff responses to rainfall. Two primary response types were identified based on the
236 number and shape of streamflow peaks: unimodal and bimodal events. Schematic diagrams
237 illustrating these three types of events are presented in Figure 2.

238 A unimodal event has a single peak generates during or shortly after the cessation of rain
239 impulse (refer to Figure 2a). While a bimodal event features two peaks as a response to the same
240 rain impulse, of which the direct peak (also called the first peak) corresponds to a fast catchment
241 response to rainfall and occurs synchronously with the rainfall or shortly after its onset.
242 Additionally, a delayed peak appears after the direct peak, exhibiting a pronounced recession that
243 can last up to several days. In cases where the delayed peak rapidly merges with the direct peak
244 into a single peak, the event is referred to as a hybrid bimodal event. Hybrid bimodal events are



245 distinguished from unimodal events by their extremely high streamflow volume, longer duration,
246 and delayed response time (Figure 2c).

247 It's worth noting that a rainfall event may consist of multiple impulses, and in such cases, the
248 hydrograph responds with multiple direct peaks (see Figure 2b). The stormflows from the first
249 peak (q_{1p}) and delayed peak (q_{2p}), along with the total event stormflow ($q_s = q_{1p} + q_{2p}$), were
250 calculated by summing hourly values over the identified event period. The runoff ratio (R_r),
251 commonly used to estimate the effective contributing area during a runoff event (Buttle *et al.*, 2004;
252 Detty & McGuire, 2010), is calculated as the ratio of q_s to gross rainfall.



253

254 **Figure 2.** Schematic diagrams of the hydrographs of an (a) unimodal event, (b) typical bimodal
255 events, and (c) hybrid bimodal event (modified from Zillgens *et al.*, 2007).

256 2.7 Definition of lag time

257 The lag time, defined as the duration between peak rainfall and peak streamflow (Mosley,
258 1979), is a critical parameter for modeling the temporal variability of streamflow. Lag time varies
259 significantly among different water sources (Becker, 2005; Haga *et al.*, 2005) and has been
260 introduced to comprehend sub-components of runoff in different response processes. In this study,
261 two specific lag times are considered: t_{1p} the time lag between peak rainfall intensity and the first
262 streamflow peak, and t_{2p} the time lag between peak rainfall intensity and the delayed streamflow
263 peak, as illustrated in Figure 3.



264 2.8 Water sampling and isotope analysis

265 Water samples for isotope analysis ($\delta^{18}\text{O}$ and δD) were collected from July 1 to September 1,
266 2021. Rainwater was automatically sampled every two hours using an ISCO6712 automatic water
267 sampler (Inc., Lincoln, Nebraska, USA) positioned near the weir. Manual bulk samples of rainfall
268 were also collected at the same location after each event using a rainwater sampler with a 9.5 cm
269 diameter funnel attached to a 500 ml plastic water bottle, insulated with bubble foil to protect
270 against direct sunlight, and a table tennis ball placed in the funnel's mouth to minimize evaporation.

271 Stream water was collected every two hours upstream of the Parshall flume location using an
272 automatic water sampler (Figure 1). Spring, seepage water, and groundwater were manually
273 collected daily from boreholes using a bailer. All collected samples underwent isotopic
274 composition analysis ($\delta^{18}\text{O}$ and δD) using a Picarro L2140-i isotopic liquid water and water vapor
275 analyzer (wavelength-scanned cavity ring-down spectroscopy, WS-CRDS) with a declared
276 precision of $\delta^{18}\text{O} \pm 0.1\text{‰}$ and $\delta\text{D} \pm 1\text{‰}$.

277 2.9 Isotopic hydrograph separation

278 To trace the source of the streamflow during storm events, a simple mass balance approach
279 was employed to segregate the streamflow into two components: event water and pre-event water.
280 These components are represented by rainfall and baseflow, respectively, based on the oxygen
281 isotopic concentration ($\delta^{18}\text{O}$) of each component. The $\delta^{18}\text{O}$ of baseflow and weighted rainwater
282 samples served as end members, defining the ultimate isotopic composition of the stream, in
283 accordance with the approach outlined by Padilla *et al.* (2014):

$$284 \quad C_s = xC_e + (1 - x)C_p \quad (2)$$

$$285 \quad x = \frac{C_s - C_p}{C_e - C_p} \cdot 100[\%] \quad (3)$$

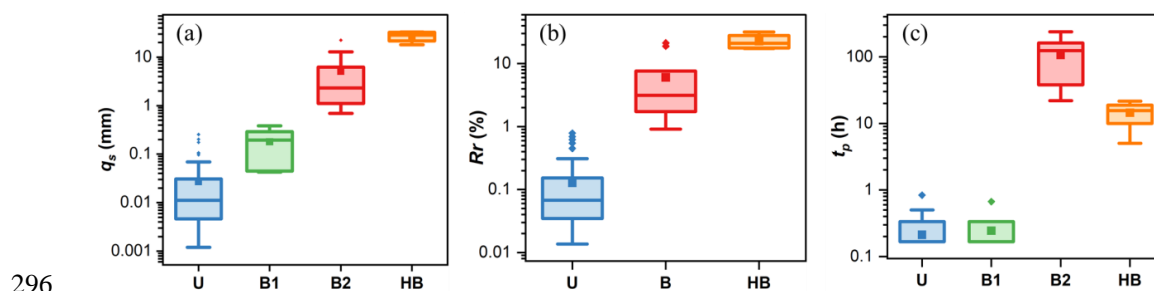


286 where C_s , C_e and C_p refer to $\delta^{18}\text{O}$ concentrations of stream, event and pre-event water components,
287 respectively. C_e is the weighted value calculated using the incremental mean weighting method
288 (McDonnell *et al.*, 1990) for each event. C_p is determined from the stream $\delta^{18}\text{O}$ concentration
289 measured immediately preceding the rainfall. x is the percentage of event water in stream.

290 3. Results

291 3.1 Characteristics of different runoff response types

292 During the period from 2014 to 2023, a total of 95 distinct rainfall events, each with a
293 cumulative rainfall of at least 5 mm, were identified from the rainfall data series. Among these
294 events, 14 exhibited a bimodal response, and an additional 4 displayed a hybrid bimodal process
295 (refer to Table 1).



296
297 **Figure 3.** Comparison of (a) stormflow, q_s , (b) runoff ratio, Rr and (c) lag time (t_p) from peak
298 rainfall to peak streamflow of different event types. U indicates unimodal event, B (including the
299 first peak B1 and the delayed peak B2) bimodal event and HB hybrid bimodal event. In each
300 boxplot, the lower and upper limits represent the lower and upper quartiles, while the whiskers
301 extend to the minimum and maximum values in each dataset. The horizontal line within the box
302 signifies the median. Individual asterisks denote points more than 1.5 times away from the median.
303 It's noteworthy that a semi-logarithmic coordinate was utilized for enhanced interpretability due
304 to the extensive range.

305 The stormflow volume and lag times of streamflow peaks for both unimodal and bimodal
306 events were determined and characterized. As depicted in Figure 3, unimodal events generated
307 relatively minimal runoff, with a maximum q_{1p} of 0.25 mm. In contrast, the q_{1p} and q_{2p} of bimodal



308 events exhibited a wider range, spanning from 0.03 to 0.38 mm and from 0.82 to 31.63 mm,
309 respectively (Figure 3b). The stormflow volume of bimodal events proved to be 3 to 114 times
310 larger than that of unimodal events, primarily due to the presence of delayed peaks (Figure 3a).
311 Correspondingly, bimodal events displayed higher Rr values ranging from 0.91% to 31.81%,
312 whereas the Rr of unimodal events remained below 0.8% (Figure 3b). This discrepancy suggests
313 an expanded effective contributing area during bimodal and hybrid bimodal events, as highlighted
314 in previous studies (Zhang *et al.*, 2021).

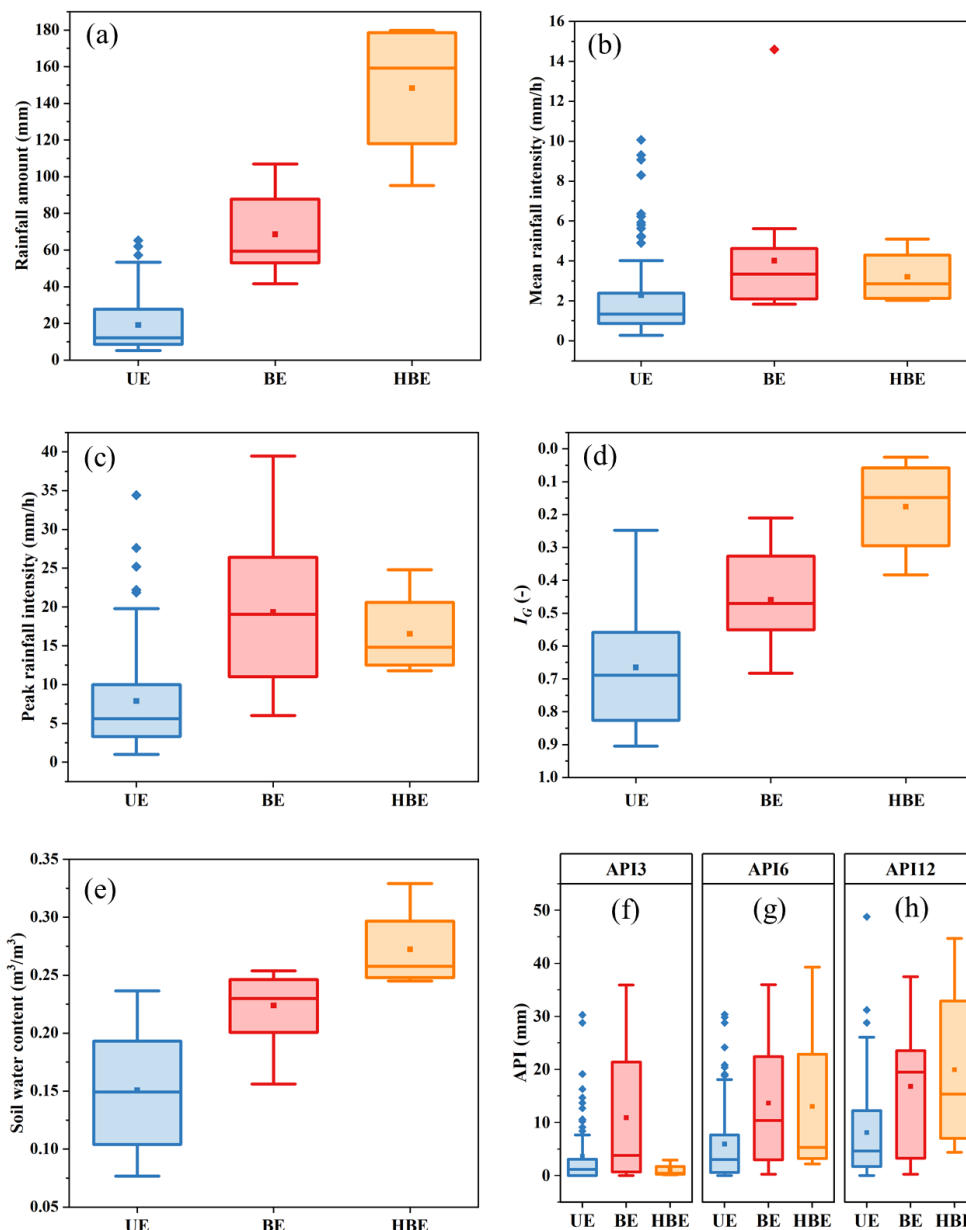
315 In both unimodal and bimodal events, all direct peaks were observed within a one-hour
316 timeframe. However, the delayed peak, a distinctive feature of bimodal events, manifested itself
317 between 5 hours and 9.9 days after the occurrence of the direct peak. Notably, hybrid bimodal
318 events exhibited shorter lag times and significantly higher stormflow yield, underscoring the need
319 for heightened attention in flood forecasting. The substantial difference in lag time strongly implies
320 that these peaks are contributed by distinct water sources, aligning with findings from previous
321 studies (Haga *et al.*, 2005).

322 **3.2 Determinants of delayed streamflow peaks**

323 The relationships between different event types and rainfall characteristic parameters and
324 watershed wetness indicators were further depicted in Figure 4. Rainfall amount, groundwater
325 level index (I_G), and soil water content (SWC) were statistically significantly different for both
326 groups, as proven by the t-test of equality of medians at a significance level of $\alpha=0.01$. The
327 transition from unimodal to bimodal events reveals a consistent increase in rainfall amount, I_G , and
328 SWC. Nearly all bimodal events exhibited rainfall amounts exceeding 50 mm, whereas the range
329 for unimodal events varied from 5.2 to 66.6 mm (Figure 4a). This suggests that the initiation of
330 delayed streamflow peaks may be associated with substantial rainfall.



331 The I_G and SWC of bimodal events, especially hybrid bimodal events, were significantly
332 higher ($p < 0.01$) than those of unimodal events. Despite partial overlap in the ranges of I_G and
333 SWC for these groups (Figure 4d and e), the mean I_G and SWC values for bimodal events (0.46
334 and 0.67) were notably greater than those for unimodal events (0.22 and 0.13), underscoring the
335 distinctiveness of these parameters between event types. Contrastingly, peak rainfall intensity,
336 mean rainfall intensity, and Antecedent Precipitation Index (API) metrics (API3, API6, and API12)
337 exhibited a widespread overlap in their variation ($p > 0.05$, Figure 4b, d, g-i). Consequently, while
338 bimodal events were characterized by higher rainfall and antecedent wetness, I_G and SWC emerged
339 as more effective indicators for estimating the occurrence of bimodal events, while peak rainfall
340 intensity, mean rainfall intensity, and API were found to be insufficient for distinguishing between
341 bimodal and unimodal events.

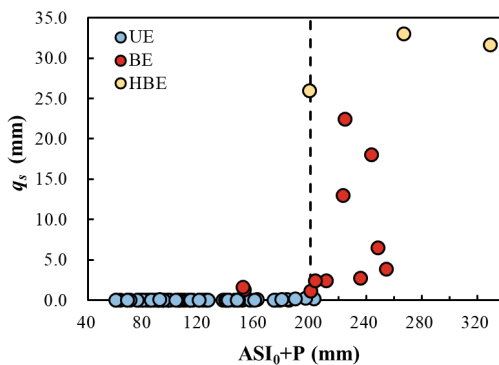


342
 343 **Figure 4.** Box plots of the hydrological characteristic parameters for unimodal and bimodal events.
 344 (a) rainfall amount; (b) mean rainfall intensity; (c) peak rainfall intensity; (d) I_G : groundwater level
 345 index; (e) soil water content; (g)-(i) API3, API6 and API12: antecedent precipitation index over 3,
 346 6 and 12 days. UE, BE and HBE are respectively unimodal, bimodal and hybrid bimodal events.
 347 To be noted, each element of the box carries the same interpretation as described in Figure 3.

348



349 Considering the interdependence of groundwater level, streamflow, and SWC on rainfall, a
350 detailed examination of the relationship between rainfall amount and bimodal events was
351 conducted. The analysis revealed that the occurrence of delayed peaks is contingent on both event
352 rainfall and antecedent wetness, displaying a distinct threshold behavior (Figure 5b). The
353 combined sum of event rainfall amount (P) and antecedent soil moisture index prior to the rainfall
354 (ASI_0) serves as a reliable indicator for predicting the occurrence of delayed peaks. Figure 5
355 illustrates that bimodal events tend to manifest when $P + ASI_0$ exceeds 200 mm (with only two
356 bimodal events misplaced). An intriguing observation is that these misplaced bimodal events
357 produced very little q_s , and these three unimodal events nearby to the threshold, occurred just
358 before the year's first bimodal response when the watershed was sufficiently humid, signaling a
359 predisposition for bimodal events. However, once the rainfall surpassed the threshold, all bimodal
360 episodes were randomly distributed, and no discernible relationship was observed between their
361 stormflow volume (q_s) and rainfall amount. Based on these findings, we posit that the stormflow
362 generation process may be dominated by groundwater or SWC.



363

364 **Figure 5.** Relationship between the $ASI_0 + P$ and stormflow volumes (q_s) of different event types.
365 UE is unimodal event, HBE is hybrid bimodal event, P is rainfall amount, and ASI_0 is antecedent
366 soil moisture index before the rainfall.

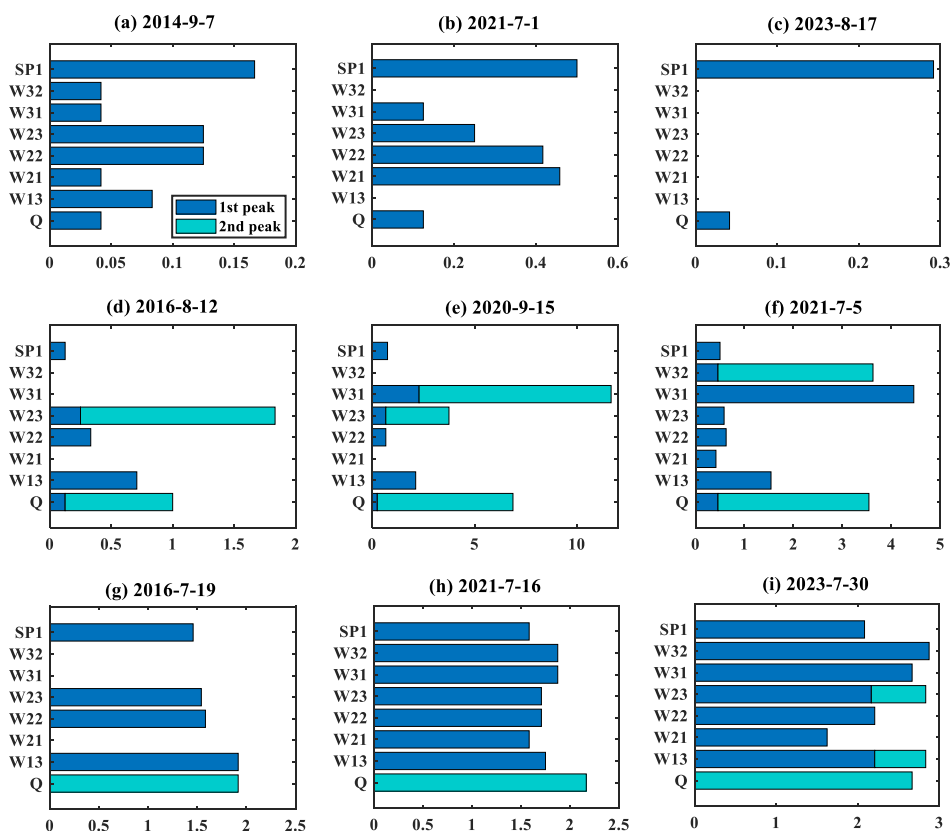
367



368 **3.3 Timing of groundwater, soil water, and streamflow response**

369 The preceding analysis indicates a correlation between different event types and groundwater
370 levels along with SWC. Moreover, the inconsistent response time among different event types may
371 signify distinct contributing sources to the stream channel, providing insights into the primary
372 mechanisms behind runoff generation. Earlier or identical response timing of groundwater
373 compared with streamflow suggested that streamflow response was driven by hillslope
374 groundwater (Haught and Meerveld, 2011; Rinderer *et al.*, 2016). To explore this further, six
375 bimodal events with minimal or sporadic rainfall during the delayed peak period, along with three
376 unimodal events, were selected. The response timing of groundwater, SWC, and streamflow is
377 illustrated in Figure 6. Each horizontal bar represents the onset of rain on the left end and the lag
378 time for the peak value on the right end of the corresponding variable. It's worth noting that some
379 groundwater levels in Figures 6d, e, and g lack horizontal bars due to missing groundwater level
380 data, while the groundwater levels in Figure 6c lack horizontal bars due to no response from
381 groundwater.

382 SWC reached their maximum after direct streamflow peaks but before delayed peaks.
383 Particularly in typical bimodal events, SWCs peaked much earlier than delayed streamflow peaks,
384 suggesting that, in these events, soil water did not contribute to direct peak but may to delayed
385 streamflow peaks. Regarding groundwater levels, some locations showed two peaks and not all
386 responded to the same rainfall event. Among different locations, groundwater levels peaked before
387 or after the delayed streamflow peaks. However, for the hybrid bimodal events, the response time
388 of groundwater levels at various locations, and even the SWC tended to coincide with the delayed
389 streamflow peak. Identical response timing or groundwater rising and peaking just before the
390 stream suggest that groundwater may be the major contribution of delayed stormflow.



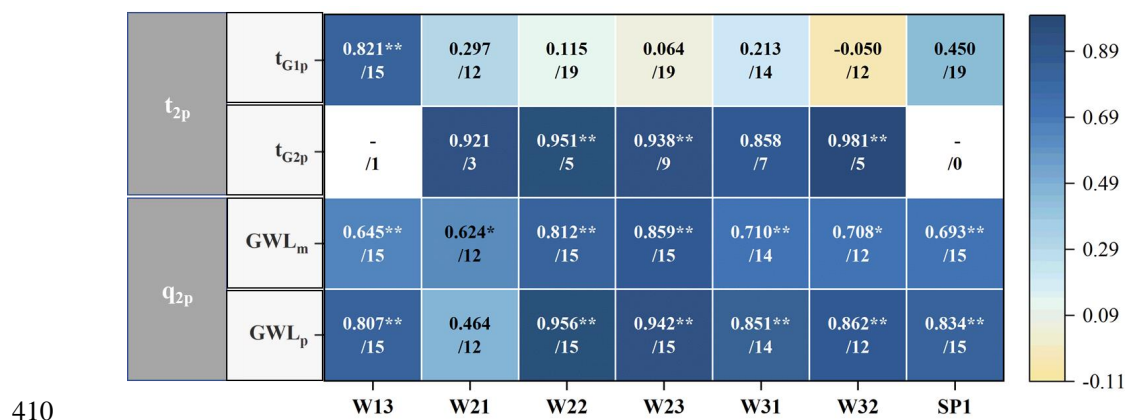
391

392 **Figure 6.** Response time of streamflow, groundwater and soil water in nine events. The horizontal
 393 axis represents the lag time from the onset of rain (days). The lengths of the bars represent the time
 394 lag for volumetric water content and groundwater level to reach the maximums from rainfall onset.

395 Pearson correlation coefficients (r_p) between peak groundwater levels, peak SWC and
 396 delayed streamflow were calculated for 19 bimodal events. As showed in Figure 7, the first two
 397 lines show the correlation coefficients between t_{2p} and the lag time of the peak groundwater levels
 398 and SWC, t_{G1p} and t_{G2p} represent the response times of the first and second peaks of groundwater
 399 level or SWC, respectively. The last two lines show the correlation coefficients between q_{2p} and
 400 the average and peak values of groundwater levels and SWC. The number after the slash specifies
 401 how many pairs of the variables.



402 Groundwater levels exhibited two peaks in some events, with the exception of W13.
 403 Correspondingly, among these events, the response time of the second peak of groundwater level
 404 has a strong correlation with t_{2p} with the $r_p > 0.858$. Even though W13's groundwater level only
 405 has one peak, this peak's response time was highly correlated with t_{2p} at the 0.01 significance level
 406 ($r_p = 0.821$). In contrast, SWC displayed one peak in all events, and its response time exhibited a
 407 weak correlation with t_{2p} ($r_p = 0.450$). Both groundwater levels and SWC, particularly their peak
 408 values, demonstrated a high correlation with delayed stormflow volumes (q_s). Above all,
 409 groundwater is deemed to be the primary controlling factor in delayed stormflow.



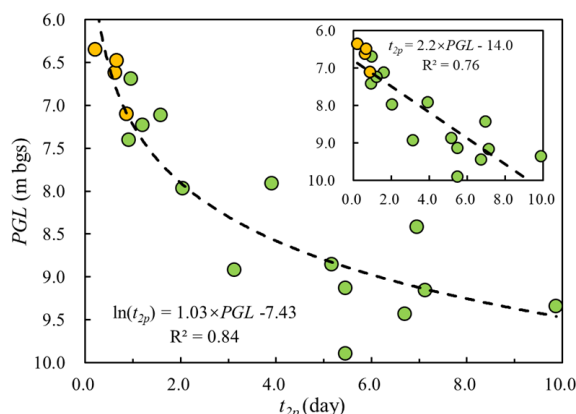
411 **Figure 7.** Pearson correlation coefficients between peak streamflow and peak groundwater levels.
 412 The number after the slash specifies how many pairs of the variables. I_G , groundwater water level
 413 index; ** Denotes that correlation is significant at the 0.01 level (two-tailed).

414 The robust correlation observed between groundwater levels at different locations and
 415 stormflow suggests that groundwater observations at a specific location can serve as a
 416 representative proxy for the overall groundwater level across the watershed. Given the relatively
 417 complete and dynamic water level observation data for W23, this borehole was selected for further
 418 analysis (Figure 7c).



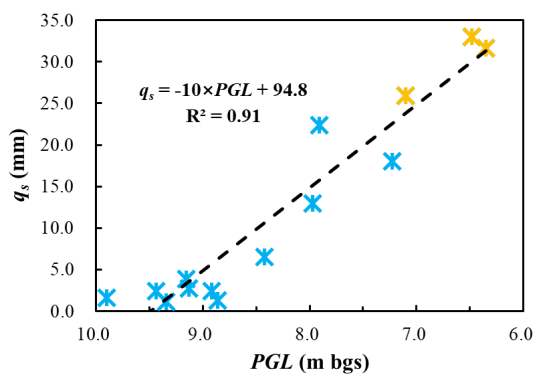
419 3.4 Stormflow timing and magnitude characteristics

420 Considering the high correlation between streamflow and groundwater level as indicated in
421 the previous analysis, we hypothesized a connection between groundwater and delayed stormflow.
422 To elucidate this correlation between groundwater and streamflow, we fitted the relationship
423 between the groundwater level at location W23 and the magnitude and timing of the delayed
424 stormflow for bimodal events. The time lag of delayed peak (t_{2p}) shows a negative exponential
425 correlation with peak groundwater level ($\ln(t_{2p}) = 1.03PGL - 7.43$, $R^2 = 0.84$, $p < 0.01$, Figure 8),
426 suggesting that a higher groundwater level corresponds to a faster response of the delayed runoff
427 peak to rainfall. A comparable linear correlation was also fitted between t_{2p} and groundwater level,
428 albeit with a slightly lower R^2 .



429
430 **Figure 8.** Correlation between peak groundwater level (PGL) and lag time of the delayed
431 streamflow peak (t_{2p}). The insert shows the same plot with linear fitting. Orange solid circles
432 represent hybrid bimodal events.

433 Moreover, as shown in Figure 9, q_s also has a strong linear relationship with groundwater
434 level ($q_{sv} = -10 \times PGL + 94.8$, $R^2 = 0.91$, $p < 0.01$). These results highlight the significant influence
435 of groundwater on flood generation in the studied watershed, suggesting that incorporating
436 groundwater level variations into flood forecasting models could enhance their accuracy.



437

438 **Figure 9.** Correlation between mean groundwater (MGL) level and stormflow amount (q_s) for
439 bimodal events. Orange stars represent hybrid bimodal events.

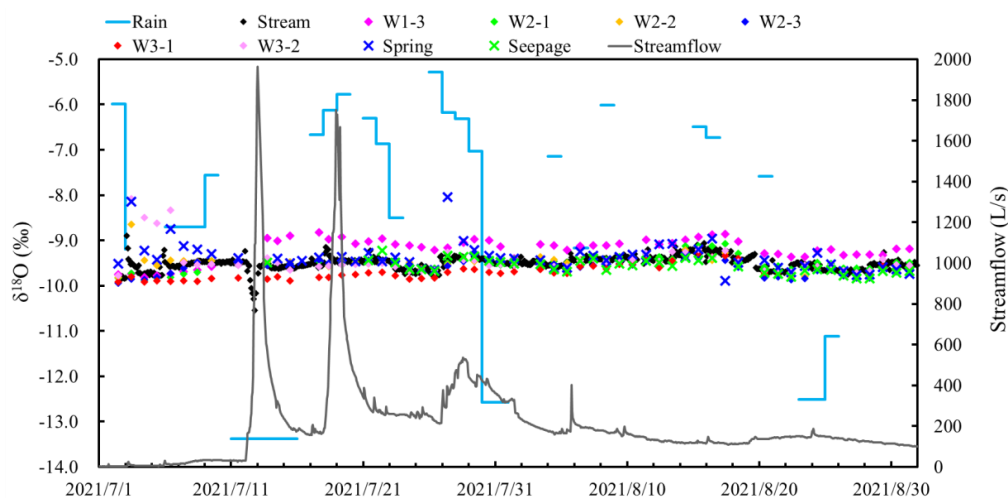
440 For both fitted lines, the closely matching fitting lines for hybrid bimodal events support the
441 hypothesis that these high, delayed streamflow responses, which may appear unimodal, are, in fact,
442 bimodal. During hybrid bimodal events, the delayed peak increased rapidly and reached its peak
443 within one day, practically merging with the direct peak. This led to a potentially misleading result
444 that only one peak was generated. This occurrence was likely due to the groundwater level rising
445 rapidly to a critical level with substantially higher hydraulic conductivity, allowing a larger portion
446 of the hillslope to become hydraulically connected to the stream during these events within a very
447 short time. Consequently, a substantial amount of groundwater was quickly discharged into the
448 channel.

449 3.5 Isotope composition of groundwater and stream water

450 To gain additional insight into the control of groundwater level on delayed stormflow, the
451 isotope compositions of different water bodies were analyzed. Figure 10 summarizes the $\delta^{18}\text{O}$ of
452 stream, spring, seepage water and the groundwater $\delta^{18}\text{O}$ from all boreholes between July 1 and
453 September 1 in 2021. Rainwater exhibited a high variation in $\delta^{18}\text{O}$ composition (ranging from -
454 14.42 to -5.28 ‰), with a rainfall-weighted mean $\delta^{18}\text{O}$ value of -9.197. In contrast, groundwater



455 $\delta^{18}\text{O}$ composition appeared more stable throughout the sampling period, showing little variation
456 across various boreholes, with a mean $\delta^{18}\text{O}$ value ranging from -9.76 ± 0.10 to $-9.08\pm 0.86\text{‰}$. This
457 stability indicates minimal event-based mixing with rainwater. The $\delta^{18}\text{O}$ values of spring and
458 seepage water followed a pattern similar to that of groundwater. The average $\delta^{18}\text{O}$ value of the
459 stream (-9.51‰) closely resembled that of groundwater (-9.49‰). Although the stream's $\delta^{18}\text{O}$
460 composition briefly deviated toward that of rainfall during a storm, it quickly reverted to its
461 previous value, resembling groundwater. Large isotopic variation in rainfall was dampened in the
462 stream, indicating that both baseflow and some stormflow originated from groundwater storage
463 with a consistent isotopic ratio, a result of dispersion and mixing processes.



464
465

Figure 10. Stable isotope $\delta^{18}\text{O}$ time series of rainfall, streamflow and groundwater.

466

467

468

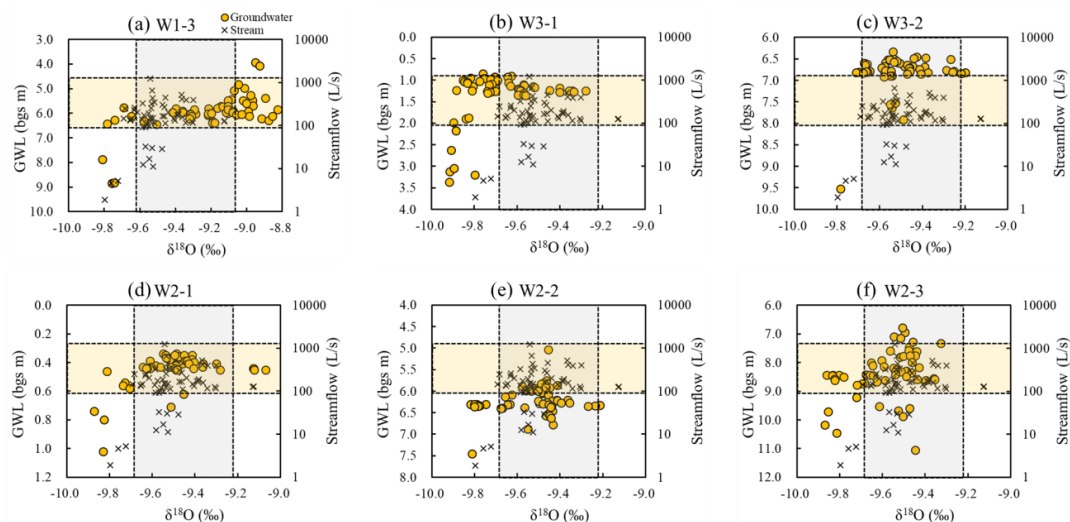
469

470

In Figure 11, groundwater $\delta^{18}\text{O}$ values were plotted against groundwater levels for each borehole, and stream water $\delta^{18}\text{O}$ values were plotted against streamflow. The variability of groundwater $\delta^{18}\text{O}$ increased with rising groundwater levels, suggesting a stronger influence of rainwater on groundwater. Stream water's $\delta^{18}\text{O}$ remained independent of streamflow volume and exhibited a range of variation similar to that of groundwater. Notably, the overlapping isotopic



471 compositions, including those during stormflow, were predominantly found in regions with higher
472 groundwater levels. This observation underscores that, even during stormflow events, groundwater
473 remains the primary source of streamflow.



474

475 **Figure 11.** $\delta^{18}\text{O}$ measurements in groundwater and stream water from July 1 to September 1, 2021.
476 Circles and cross represent the $\delta^{18}\text{O}$ of groundwater and stream water, respectively.

477 4. Discussion

478 4.1 Lag time of delayed streamflow peaks

479 The lag time of delayed peaks varies across different water sources, providing valuable
480 insights for estimating stormflow water resources. Haga *et al.* (2005) conducted relevant studies
481 in a forested unchanneled catchment, noting that events with shorter lag times (<2 hours)
482 predominantly exhibited runoff composed of saturation excess overland flow near the spring area.
483 In contrast, events with longer lag times (>24 hours) were characterized by river runoff mainly
484 composed of saturated subsurface flow above the soil-bedrock interface. Becker (2005)
485 synthesized lag times from various studies in different basins, observing a trend where lag times



486 for the three main flow components differed by at least one order of magnitude, following the
487 pattern overland flow < subsurface flow < baseflow. This substantial difference in lag times is
488 likely attributed to the stochastic triggering of different flow paths by rainfall forcing in distinct
489 events.

490 Lag times of the direct streamflow peaks for both unimodal and bimodal events were
491 generally within 30 min in this study, which had no significant correlation with rainfall amount,
492 rainfall intensity, or pre-event streamflow with the correlation coefficients were 0.005, 0.017 and
493 0.012, respectively, indicating the direct streamflow peak was nearly concurrent with the rainfall.
494 Therefore, we could infer that the direct peaks were generated by bypass flow via macropores,
495 fractures or soil-bedrock interface (Buttle and Turcotte, 1999; Onda *et al.*, 2001; Uchida *et al.*,
496 2005; Xu *et al.*, 2016), or contributed by the direct rainfall into the channel considering that 1 h
497 was roughly the routing time of river network in XEW (Zhao *et al.*, 2019).

498 Lag times for the direct streamflow peaks, observed in both unimodal and bimodal events in
499 this study, were generally within 30 minutes. These lag times exhibited no significant correlation
500 with rainfall amount, rainfall intensity, or pre-event streamflow (correlation coefficients of 0.005,
501 0.017, and 0.012, respectively). This lack of correlation suggests that the direct streamflow peaks
502 were nearly concurrent with rainfall. Therefore, we infer that these direct peaks were generated
503 either through bypass flow mechanisms, such as macropores, fractures, or soil-bedrock interfaces,
504 as interpreted in Buttle and Turcotte (1999), Onda *et al.* (2001), Uchida *et al.* (2005), and Xu *et al.*
505 (2016). Alternatively, they could have been directly contributed to the channel by rainfall. This
506 interpretation aligns with the consideration that the routing time of the river network in XEW is
507 approximately 1 hour (Zhao *et al.*, 2019).



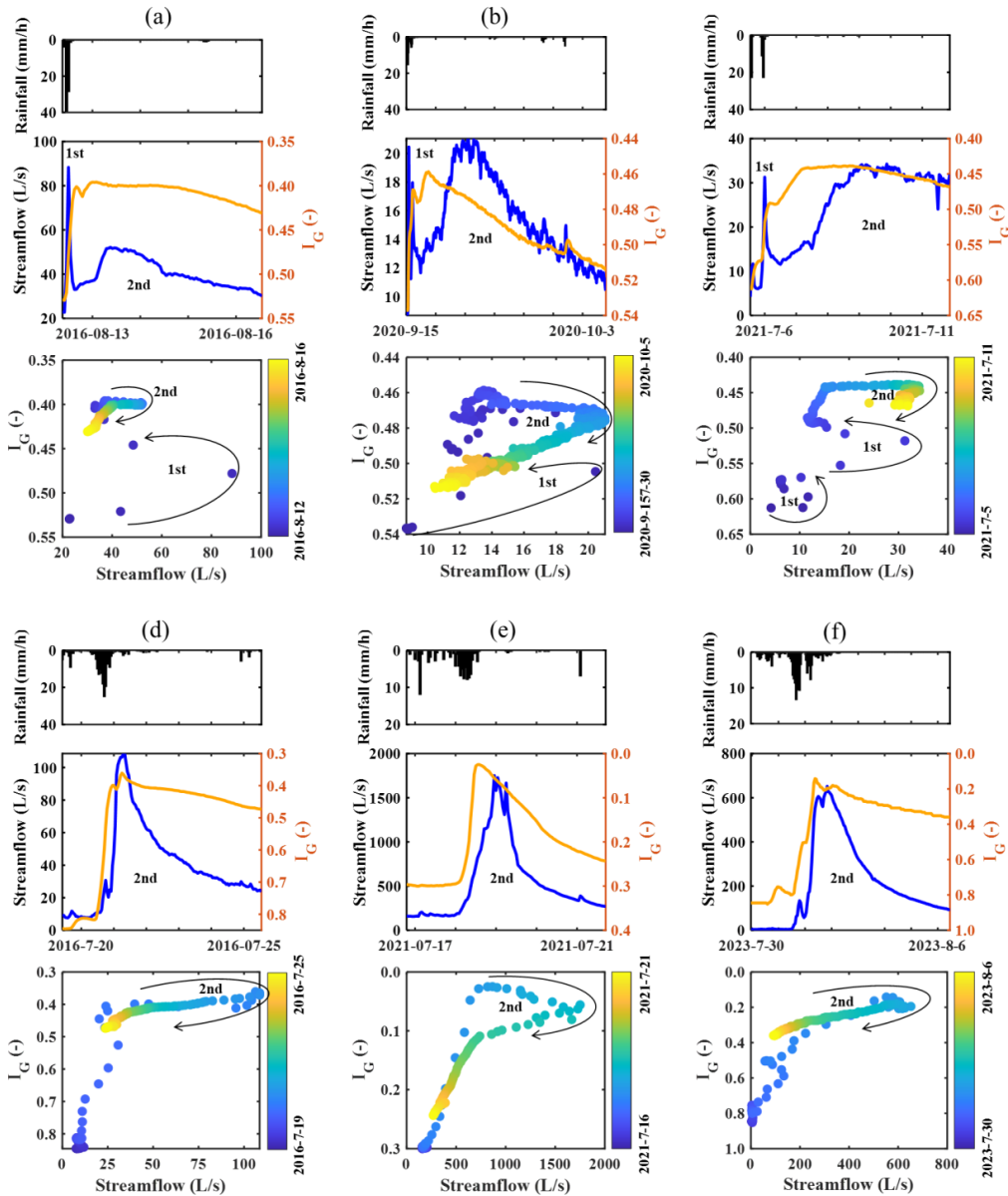
508 In contrast to the direct peaks, the time lags from the peak rainfalls to the delayed peaks were
509 considerably longer, ranging from 5 hours to 9.9 days (Figure 3). This lag time in our study aligns
510 with findings from other studies where similar parameters were calculated (refer to Table 3). The
511 results imply that the delayed peaks observed in XEW were likely generated by subsurface flow
512 processes, as indicated in the work of Lischeid *et al.* (2002).

513 **Table 3.** Lag time between peak rainfall intensity and the delayed streamflow peak in this study
514 and in previous studies

Reference	Lag time of delayed peak	The source of the delayed peak
Onda <i>et al.</i> (2001)	Ten hours to one week	Subsurface flow and bedrock groundwater
Zillgens <i>et al.</i> (2007)	Three to five days	Subsurface flow
Padilla <i>et al.</i> (2014, 2015)	Within four days	Bedrock groundwater
Masiyandima <i>et al.</i> (2003)	Several hours	Subsurface flow
Anderson & Burt (1978)	About one day	Subsurface flow
This study	5 hours to 9.9 days	Subsurface flow (groundwater flow)

515 4.2 Hysteresis between groundwater level and streamflow

516 For bimodal events in XEW, the non-linear relationship between groundwater level and
517 streamflow results in hysteretic relationships between the two variables. Figure 11 shows time
518 series for streamflow and I_G as well as scatter plots comparing the two variables for the six events
519 used in section 3.3. As noted by Dunne (1978), when two runoff peaks appeared in an event, there
520 must be at least two zones in the catchment that responded to the storm and contributed to runoff.
521 The hysteretic nature highlights the possibility of multiple hydrological compartments being active
522 and these compartments are not necessarily contributing significant flows simultaneously but
523 rather sequentially during the runoff generation period (Fovet *et al.*, 2015; Martínez-Carreras *et*
524 *al.*, 2016).



525

526

527

528

529

530

531

Figure 11. Streamflow and I_G with corresponding scatter plots between both variables for three typical bimodal and three hybrid bimodal events. Note that the axis scales vary between events. Arrows indicate progression of time. Direct peaks in bimodal hydrographs indicated as “1st” and delayed peaks as “2nd”.



532 Streamflow increased quickly and peaked before groundwater level during direct peaks,
533 resulting in an anti-clockwise hysteretic loop. It can be explained that direct peaks were formed by
534 rainfall directly falling onto the channel or a saturation zone near the channel, and/or by the flow
535 that contributed to the channel through rapid routes, as observed in other watersheds by Jackisch
536 *et al.* (2016). In contrast, groundwater level peaked first during delayed peaks, indicating that the
537 groundwater level in the watershed peaked first and subsequently released water, creating the
538 delayed runoff peak. This behavior may be attributed to the groundwater level surpassing a
539 threshold for generating bimodal hydrographs, leading to enhanced hydraulic connectivity
540 between hillslopes and the channel. This, in turn, resulted in the swift release of a substantial
541 amount of groundwater or subsurface flow (Burt & Butcher, 1985; Detty and McGuire, 2010;
542 McGlynn & McDonnell, 2003; McGuire and McDonnell, 2010; Scaife and Band, 2017).
543 Consequently, the groundwater level is not merely a passive feature in this watershed, where
544 shallow groundwater may constitute the primary runoff component, but actively controls the
545 stormflow.

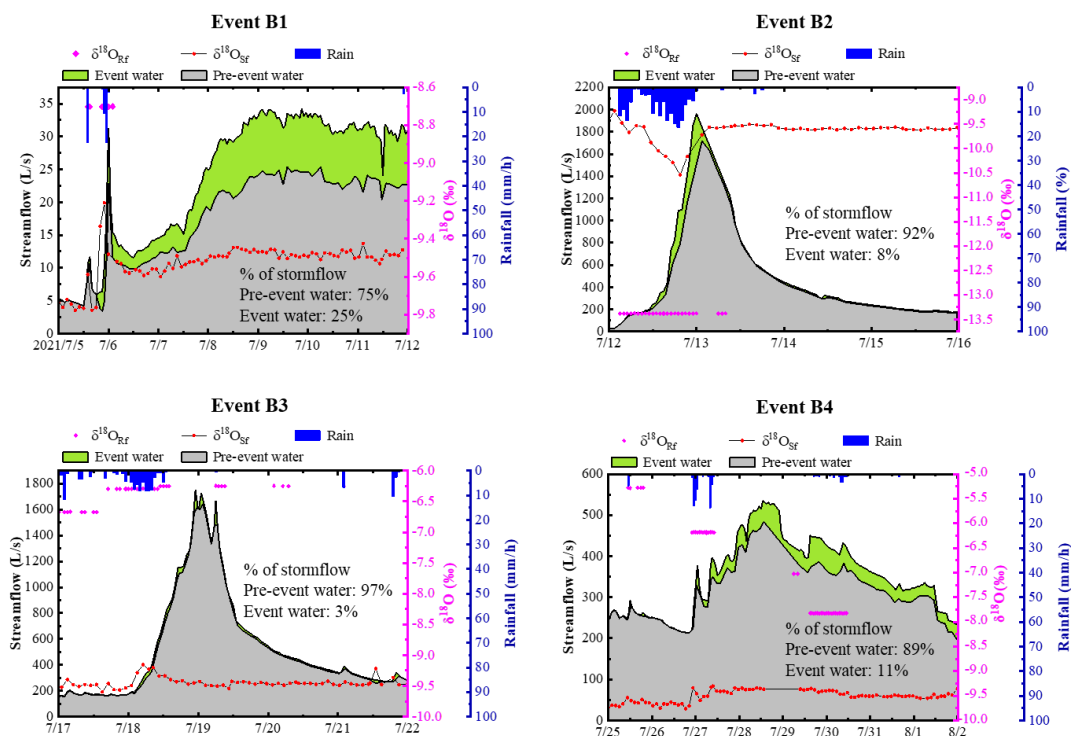
546 **4.3 Two-component hydrograph separation**

547 The two-component hydrograph separation was performed for four bimodal storm events
548 using the $\delta^{18}\text{O}$ of the bulk rainfall, a pre-event water signature (represented by the stream $\delta^{18}\text{O}$
549 before the rainfall) and the monitored stream water signature during the events. These four events
550 were chosen because their relatively complete isotope data. It should be noted that in all four
551 rainfall events, $\delta^{18}\text{O}$ values in rain and stream water were notably different, which is a requirement
552 for end-member hydrograph separation analysis. The hydrograph separation results, as well as the
553 $\delta^{18}\text{O}$ series of rainwater and stream water were shown in Figure 12.



554 Regarding the water sources separation result, these four events can be divided into two
555 groups: Event B1 and B4, the major stormflow process were lagged and considerably damped, and
556 event water contributions were higher compared to the other two events. The fraction of event
557 water comprising the hydrograph was 25% in Event B1, and the contribution ratio of event water
558 in Event 4 was 11%. Considering that the rain had already stopped, the event water component of
559 the delayed peak should be the rainwater temporarily stored in the watershed during the rainfall
560 process. Event B2 and especially Event B3, however, were almost entirely pre-event water
561 dominated (the contributions of pre-event water were 92% for Event 2 and 97% for Event B3),
562 although it was evident that some event water contributed to the stormflow during the rising and
563 peak period of streamflow, this water may have originated from the direct rainfall or rain water
564 taking a rapid route to the stream channel.

565 The hydrograph separation results indicated that the streamflow contribution of pre-event
566 water changed virtually in sync with streamflow following the onset of rain, almost entirely
567 dominating the hydrograph, while event water dominated the sharp streamflow peak responding
568 to high-intensity storm. Early in the rainy event, the pre-event component of the hydrograph
569 exceeded 50%, indicating a sufficiently swift groundwater response such that considerable
570 amounts of groundwater were released soon after the start of rain.



571
572 **Figure 12.** The partitioning of stormflow into its pre-event and event water sources using one-
573 tracer two component hydrograph separation analysis with $\delta^{18}\text{O}$ as tracer for the four storm
574 events. $\delta^{18}\text{O}_{\text{Rf}}$ and $\delta^{18}\text{O}_{\text{Sf}}$ are the $\delta^{18}\text{O}$ respectively for rain and stream water.

575 In addition, there was a noticeable, gradual rise in the pre-event water contribution to total
576 stormflow as the catchment was wetting-up (Figure 12). Event B1 had a rather dry antecedent
577 condition and showed a relatively lower pre-event water percentage (about 75%). Event 3 in the
578 temporal sequence had a extremely high pre-event water proportion (approximately 97%) and
579 occurred under highly wet antecedent conditions. In Event B4, due to a little reduced wetness
580 condition compared to the preceding Event B3, the percentage of pre-event water decreased
581 somewhat to approximately 89%. This pattern may be attributed to increased water flux during the
582 wetting-up process when the water table rose into near surface soil layers with high saturated
583 hydraulic conductivity. The rate of groundwater increase slowed as a result of the higher



584 transmissivity, and more pre-event water was mobilized and travelled rapidly to the stream via
585 shallow flow pathways (Lundin, 1982).

586 4.4 Filed observation

587 Our field observations on-site indicate that direct exfiltration of groundwater into the runoff
588 predominates, with few signs of hillslope overland flow. For example, during a heavy storm on
589 July 5, 2021, characterized by short duration (7 hours) and very high intensity (27.6 mm/h) with a
590 total rainfall of 65.2 mm, minimal overland flow was observed at the study site. However, post
591 storm on July 5, the spring water flow from Hillslope 2 substantially increased. Moreover, at
592 various points in the watershed, seepage flow was observed gushing from fractures in the stone
593 and holes in the earth. These field observations strongly suggest the direct exfiltration of
594 groundwater into the runoff, providing further support to the notion that groundwater significantly
595 contributes to stormflow in the watershed.



596

597 **Figure 14.** Field observations of the spring and the seepage flows. HS1, HS2 and HS3 are Hillslope
598 1, Hillslope 2 and Hillslope 3, respectively.

599 5. Conclusions

600 Based on observations from 2013 to 2023, the study carried out an event-scale analysis of
601 streamflow hydrographs in a semi-humid forested watershed of North China. Three stormflow



602 patterns with distinct shaped hydrograph, i.e., unimodal, bimodal, and hybrid bimodal were
603 identified. Particularly, their rainfall-runoff response characteristics as well the stormflow
604 composition were analyzed, and derived the following conclusions:

605 1) Direct peaks for both unimodal and bimodal events occurred within 1 hour following the
606 peak rainfall, while the lag time of delayed peaks ranged between 5 h and 9.9 days. The stormflow
607 amount generated by bimodal events, due to the delayed peak, was several to hundreds of times
608 more than that of the unimodal events, often resulting in flooding.

609 2) Delayed stormflow appeared when the sum of event rainfall amount (P) and antecedent
610 soil moisture index (ASI) exceeding 200 mm. Stormflow yield is positively proportional to event
611 peak groundwater level while the lag time of delayed peak showed an inverse correlation with
612 peak groundwater level.

613 3) The isotopic analysis and two-component hydrograph separation unveiled that pre-event
614 water predominantly contributed to the delayed stormflow, with event water dominating the sharp
615 streamflow peak in response to high-intensity storms.

616 4) Streamflow peaked before groundwater level during direct peaks, suggesting that direct
617 streamflow peaks are from direct rainfall onto the channel or rapid flow through macropores and
618 bedrock fractures, Discharge peaked before catchment storage during single peak. But
619 groundwater levels peaked first during delayed streamflow, suggested that the delayed stormflow
620 is primarily made up of shallow groundwater, and this is further supported by field observation.

621 This study clarified the prerequisites for bimodal stormflow, and the provided information on
622 the response characteristics and water resources of stormflow is not common knowledge for
623 regions. We believe these findings can enrich runoff generation theory and contribute new insights
624 for stormflow modelling in other similar regions.



625 **Data availability**

626 All the data used in this study will be available at the Zenodo website at the time of
627 publication.

628 **Author contribution**

629 ZC contributed the conceptualization, formal analysis, investigation and writing; FT
630 contributed the conceptualization, formal analysis and revision; ZZ, ZX, YD and JW contributed
631 the Investigation; M contributed the writing.

632 **Competing interests**

633 Some authors are members of the editorial board of Hydrology and Earth System Sciences.

634 **Financial support**

635 This study was supported by the National Key R&D Program of China (2022YFC3002902)
636 and the National Natural Science Foundation of China (51825902).

637 **Acknowledgments**

638 We acknowledge Jeffrey McDonnell for constructive advice on this study.

639 **References**

640 Ali, G., Tetzlaff, D., McDonnell, J. J., Soulsby, C., Carey, S., Laudon, H., McGuire, K., Buttle, J., Seibert, J.,
641 Shanley, J.: Comparison of threshold hydrologic response across northern catchments. *Hydrological*
642 *Process*, 29 (16), 3575–3591, doi:10.1002/hyp.10527, 2015.



- 643 Anderson, M. G. and Burt, T. P.: Automatic monitoring of soil moisture conditions in a hillslope spur and hollow.
644 *Journal of Hydrology*, 33(1–2), 0–36, doi:10.1016/0022-1694(77)90096-8
- 645 Anderson, M. G. and Burt, T. R. (1978). The role of topography in controlling throughflow generation. *Earth*
646 *Surface Processes*, 3(4), 331–334, doi:10.1002/esp.3290030402, 1977.
- 647 Becker, A.: Runoff Processes in Mountain Headwater Catchments: Recent Understanding and Research
648 Challenges. *Global Change and Mountain Regions*, 283–295, doi:10.1007/1-4020-3508-x_29, 2005.
- 649 Becker, A. and McDonnell, J. J.: Topographical and ecological controls of runoff generation and lateral flows in
650 mountain catchments. *IAHS Publications-Series of Proceedings and Reports-Intern Assoc Hydrological*
651 *Sciences*, 248, 199-206, 1998.
- 652 Burt, T. P. and Butcher, D. P.: Topographic controls of soil moisture distributions. *Journal of Soil Science*, 36(3),
653 469–486, doi:10.1111/j.1365-2389.1985.tb00351.x, 1985.
- 654 Buttle, J. M., Dillon, P. J., and Eerkes, G. R.: Hydrologic coupling of slopes, riparian zones and streams: An
655 example from the Canadian Shield, *Journal of Hydrology*, 287(1–4), 161–177,
656 doi:10.1016/j.jhydrol.2003.09.022, 2004.
- 657 Buttle, J. M. and Turcotte, D. S.: Runoff processes on a forested slope on the Canadian Shield. *Hydrology*
658 *Research*, 30(1), 1-20, doi:10.1016/S0304-2995(99)80027-8, 1999.
- 659 Detty, J. M. and Mcguire, R. J. Threshold changes in storm runoff generation at a till-mantled headwater
660 catchment. *Water Resources Research*, 46(7), 759–768, doi:10.1029/2009wr008102, 2010.
- 661 Dingman, S. L.: *Physical hydrology*. Long Grove, IL: Waveland Press, 2015.
- 662 Dubreuil, P. L.: *Etude hydrologique de petits bassins en Cote d’Ivoire*. Rapport general. ORSTOM Service
663 Hydrologique, 1960.
- 664 Dubreuil, P. L.: Review of field observations of runoff generation in the tropics. *Journal of Hydrology*, 80(3-4),
665 237–264, doi:10.1016/0022-1694(85)90119-2, 1985.
- 666 Dunne, T.: Field studies of hillslope flow processes. In M. J. Kirkby (Eds.), *Hillslope Hydrology* (pp. 227–293).
667 London, Wiley, 1978.



- 668 Fovet, O., Ruiz, L., Hrachowitz, M., Faucheux, M., and Gascuel-Oudou, C.: Hydrological hysteresis and its
669 value for assessing process consistency in catchment conceptual models. *Hydrology and Earth System*
670 *Sciences*, 19(1), 105-123, doi:10.5194/hess-19-105-2015, 2015.
- 671 Fu, C., Chen, J., Jiang, H., and Dong, L.: Threshold behavior in a fissured granitic catchment in southern China:
672 1. Analysis of field monitoring results. *Water Resources Research*, 49(5), 2519–2535,
673 doi:10.1002/wrcr.20191, 2013.
- 674 Graeff, T., Zehe, E., Reusser, D., Lück, E., Schröder, B., Wenk, G., John, H., and Bronstert, A.: Process
675 identification through rejection of model structures in a mid-mountainous rural catchment: observations of
676 rainfall-runoff response, geophysical conditions and model inter-comparison. *Hydrological Processes*,
677 23(5), 702–718, doi:10.1002/hyp.7171, 2009.
- 678 Gu, W.: On the hydrograph separation traced by environmental isotopes. *Advances in Water Science*, 7(2): 105–
679 111, 1996.
- 680 Haga, H., Matsumoto, Y., Matsutani, J., Fujita, M., Nishida, K., and Sakamoto, Y.: Flow paths, rainfall properties,
681 and antecedent soil moisture controlling lags to peak discharge in a granitic unchanneled catchment. *Water*
682 *Resources Research*, 41(12), 2179–2187, doi:10.1029/2005wr004236, 2005.
- 683 Iwagami, S., Tsujimura, M., Onda, Y., Shimada, J., and Tanaka, T.: Role of bedrock groundwater in the rainfall-
684 runoff process in a small headwater catchment underlain by volcanic rock. *Hydrological Processes*, 24(19),
685 2771–2783, doi:10.1002/hyp.7690, 2010.
- 686 Jackisch, C., Angermann, L., Allroggen, N., Sprenger, M., Blume, T., Weiler, M., Tronicke, J., and Zehe, E.: In
687 situ investigation of rapid subsurface flow: identification of relevant spatial structures beyond heterogeneity.
688 *Hydrology and Earth System Sciences Discussions*, 1–32, doi:10.5194/hess-2016-190, 2016.
- 689 Jenkins, A., Ferrier, R. C., Harriman, R., and Ogunkoya, Y. O.: A case study in catchment hydrochemistry:
690 Conflicting interpretations from hydrological and chemical observations, *Hydrological Processes*, 8(4),
691 335–349, doi:10.1002/hyp.3360080406, 1994.



- 692 Kosugi, K., Fujimoto, M., Katsura, S., Kato, H., Sando, Y., & Mizuyama, T.: Localized bedrock aquifer
693 distribution explains discharge from a headwater catchment. *Water Resources Research*, 47(7),
694 doi:10.2929/2010WR009884, 2011.
- 695 Lischeid, G., Kolb, A., and Alewell, C.: Apparent transitory flow in groundwater recharge and runoff generation.
696 *Journal of Hydrology*, 265(1–4), 195–211, doi:10.1016/s0022-1694(02)00108-7, 2002.
- 697 Lundin L.: Soil moisture and ground water in till soil and the significance of soil type for runoff. PhD Thesis,
698 Uppsala University, UNGI Report, 56, 216, 1982.
- 699 Martínez-Carreras, N., Hissler, C., Gourdol, L., Klaus, J., Juilleret, J., Iffly, J. F., and Pfisteret, L.: Storage
700 controls on the generation of double peak hydrographs in a forested headwater catchment. *Journal of*
701 *Hydrology*, 543, 255–269, doi:10.1016/j.jhydrol.2016.10.004, 2016.
- 702 Martínez-Carreras, N., Wetzel, C. E., Frentress, J., Ector, L., McDonnell, J. J., Hoffmann, L., Pfister, L.:
703 Hydrological connectivity inferred from diatom transport through the riparian-stream system. *Hydrology and*
704 *Earth System Sciences*, 19(7), 3133–3151, doi:10.5194/hess-19-3133-2015, 2015.
- 705 Masiyandima, M. C., van de Giesen, N., Diatta, S., Windmeijer, P. N., and Steenhuis, T. S.: The hydrology of
706 inland valleys in the sub-humid zone of West Africa: rainfall-runoff processes in the M’be experimental
707 watershed. *Hydrological Processes*, 17(6), 1213–1225, doi:10.1002/hyp.1191, 2003.
- 708 McDonnell, J. J., Bonell, M., Stewart, M. K., and Pearce, A. J.: Deuterium variations in storm rainfall:
709 Implications for stream hydrograph separation. *Water resources research*, 26(3), 455–458,
710 doi:10.1029/WR026i003p00455, 1990.
- 711 McDonnell, J. J., Sivapalan, M., Vaché, K., Dunn, S., Grant, G., Haggerty, R., Hinz, C., Hooper, R., Kirchner,
712 J., Roderick, M. L., Selker, J., Weiler, M.: Moving beyond heterogeneity and process complexity: A new
713 vision for watershed hydrology. *Water Resources Research*, 43(7), doi:10.1029/2006WR005467, 2007.
- 714 McGlynn, B. L., and McDonnell, J. J.: Quantifying the relative contributions of riparian and hillslope zones to
715 catchment runoff, *Water Resources Research*, 39(11), 1310, doi:10.1029/2003wr002091, 2003.
- 716 McGuire, K. J. and McDonnell, J. J.: Hydrological connectivity of hillslopes and streams: Characteristic time
717 scales and nonlinearities. *Water Resources Research*, 46(10), doi:10.1029/2010WR009341, 2010.



- 718 Mosley, M. P.: Streamflow generation in a forested watershed, New Zealand. *Water Resources Research*, 15(4),
719 795–806, doi:10.1029/wr015i004p00795, 1979.
- 720 Onda, Y., Komatsu, Y., Tsujimura, M., and Fujihara, J.: The role of subsurface runoff through bedrock on storm
721 flow generation. *Hydrological Processes*, 15(10), 1693–1706, doi:10.1002/hyp.234, 2001.
- 722 Padilla, C., Onda, Y., Iida, T., Takahashi, S., and Uchida, T.: Characterization of the groundwater response to
723 rainfall on a hillslope with fractured bedrock by creep deformation and its implication for the generation of
724 deep-seated landslides on Mt. Wanitsuka, Kyushu Island. *Geomorphology*, 204, 444–458,
725 doi:10.1016/j.geomorph.2013.08.024, 2014.
- 726 Padilla, C., Onda, Y., and Iida, T.: Interaction between runoff-bedrock groundwater in a steep headwater
727 catchment underlain by sedimentary bedrock fractured by gravitational deformation. *Hydrological
728 Processes*, 29(20), 4398–4412, doi:10.1002/hyp.10498, 2015.
- 729 Penna, D., Tromp-van Meerveld, H. J., Gobbi, A., Borga, M., and Dalla Fontana, G.: The influence of soil
730 moisture on threshold runoff generation processes in an alpine headwater catchment. *Hydrology and Earth
731 System Sciences*, 15(3), 689–702, doi:10.5194/hess-15-689-2011, 2011.
- 732 Phillips, J. D.: Sources of nonlinearity and complexity in geomorphic systems, *Progress in Physical Geography*,
733 27(1), 1–23, doi:10.1191/0309133303pp340ra, 2003.
- 734 Powell, D. N., Khan, A. A., Aziz, N. M., and Raiford, J. P.: Dimensionless rainfall patterns for South Carolina.
735 *Journal of Hydrologic Engineering*, 12(1), 130–133, doi:10.1061/(asce)1084-0699(2007)12:1(130), 2007.
- 736 Ross, C. A., Ali, G. A., Spence, C., and Courchesne, F.: Evaluating the Ubiquity of Thresholds in Rainfall -
737 Runoff Response Across Contrasting Environments. *Water Resources Research*, 57(1), e2020WR027498,
738 doi:10.1029/2020wr027498, 2021.
- 739 Scaife, C. I. and Band, L. E.: Nonstationarity in threshold response of stormflow in southern Appalachian
740 headwater catchments. *Water Resources Research*, 53(8), 6579–6596, doi:10.1002/2017WR020376, 2017.
- 741 Sivapalan, M.: Process complexity at hillslope scale, process simplicity at the watershed scale: Is there a
742 connection? *Hydrological Processes*, 17(5), 1037–1041, doi:10.1002/hyp.5109, 2003.
- 743



- 744 Tian, F., Li, H., and Sivapalan, M.: Model diagnostic analysis of seasonal switching of runoff generation
745 mechanisms in the blue river basin, oklahoma. *Journal of Hydrology*, 418–419, 136–149,
746 doi:10.1016/j.jhydrol.2010.03.011, 2012.
- 747 Tie, Q., Hu, H., Tian, F., Guan, H., and Lin, H.: Environmental and physiological controls on sap flow in a
748 subhumid mountainous catchment in north china. *Agricultural and Forest Meteorology*, 240–241, 46–57,
749 doi:10.1016/j.agrformet.2017.03.018, 2017.
- 750 Tromp-van Meerveld, H. J., and McDonnell, J. J.: Threshold relations in subsurface stormflow: 1. A 147-storm
751 analysis of the Panola hillslope. *Water Resources Research*, 42, W02410, doi:10.1029/2004WR003778,
752 2006,
- 753 Uchida, T., Tromp-van Meerveld, I., and McDonnell, J. J.: The role of lateral pipe flow in hillslope runoff
754 response: An intercomparison of non-linear hillslope response. *Journal of Hydrology*, 311(1-4), 117–133,
755 doi:10.1016/j.jhydrol.2005.01.012, 2005.
- 756 Westhoff, M. C., Bogaard, T. A., and Savenije, H. H. G.: Quantifying spatial and temporal discharge dynamics
757 of an event in a first order stream, using distributed temperature sensing. *Hydrology and Earth System
758 Sciences*, 15(6), 1945–1957, doi:10.5194/hess-15-1945-2011, 2011.
- 759 Weyman, D., R.: Throughflow on hillslopes and its relation to the stream hydrograph. *International Association
760 of Scientific Hydrology. Bulletin*, 15(3), 25–33, doi:10.1080/02626667009493969, 1970.
- 761 Wrede, S., Fenicia, F., Martínez-Carreras, N., Juilleret, J., Hissler, C., Krein, A., Savenije, H. H. G., Uhlenbrook,
762 S., Kavetski, D., Pfister, L.: Towards more systematic perceptual model development: a case study using 3
763 Luxembourgish catchments. *Hydrological Processes*, 29(12), 2731–2750, doi:10.1002/hyp.10393, 2015.
- 764 Xu, Q., Liu, H., Ran, J., Li, W., and Sun, X.: Field monitoring of groundwater responses to heavy rainfalls and
765 the early warning of the Kualiangzi landslide in Sichuan Basin, southwestern China. *Landslides*, 13, 1555–
766 1570, doi:10.1007/s10346-016-0717-3, 2016.
- 767 Zhang, G. T., Cui, P., Gualtieri, C., Zhang, J. L., Ahmed Bazai, N., Zhang, Z. T., Wang, J., Tang, J. B., Chen,
768 R., Lei, M. Y.: Stormflow generation in a humid forest watershed controlled by antecedent wetness and
769 rainfall amounts. *Journal of Hydrology*, 603, doi:10.1016/j.jhydrol.2021.127107, 2021.



770 Zillgens, B., Merz, B., Kirnbauer, R., and Tilch, N.: Analysis of the runoff response of an alpine catchment at
771 different scales. *Hydrology and Earth System Sciences*, 11(4), 1441–1454, doi:10.5194/hess-11-1441-2007,
772 2007.